PCCP

Accepted Manuscript

ROYAL SOCIETY OF CHEMISTRY

www.rsc.org/pccp

Defect-induced Semiconductor to Metal Transition in the Graphene Monoxide

Jungwook Woo, Kyung-Han Yun, Sung Beom Cho, Yong-Chae Chung*

Department of Materials Science and Engineering, Hanyang University, 17 Haengdang-dong, Seongdong-gu, Seoul 133-791, Republic of Korea

Abstract

This study investigates the influence of point defects in the geometric and electronic structure of graphene monoxide (GMO) via density functional theory calculations. In aspects of defect formation energy, GMOs with oxygen vacancy and bridge interstitial defect are more likely to form when compared to GMOs with defects such as carbon vacancy and hollow interstitial defect. It was also found that the oxygen vacancy or hollow interstitial defect induces local tensile strain around defective site and this strain increases the band gap energy of the defective GMO. In addition, the band gaps for GMO with carbon vacancy or bridge interstitial defects decreased mainly due to the dangling bonds, not the strain effect. It is noted that the dangling bond derived from the defects forms the defect-level in band gap of GMO. The semiconductor to metal transition by band gap change (0-0.7eV) implies the possibility for band gap engineering of GMO by vacancies and interstitial defects.

*Corresponding author. Tel.:+82-2-2296-5308; Email address: yongchae@hanyang.ac.kr

1. Introduction

Since graphene was mechanically exfoliated[1], the remarkable electronic properties of graphene have become one of the most attractive topics of research[1-3]. Because of its unprecedented electronic properties, a lot of effort has been devoted to the application of graphene in electronics[4,5]. However, the zero-gap of graphene prevents applications in electronics that require a certain band gap. To overcome the semi-metallic properties of graphene, there have been many studies such as bilayer graphene through gating effects[6], interactions with substrates[7,8], and the formation of graphene nanoribbon (GNR)[9,10], graphene quantum dot (GQD)[11] and chemically modified graphene[12].

One of the many attempts to generate a band gap of graphene is by chemically modifying graphene, such as graphene monoxide (GMO) [13]. Recently, it has been reported that graphene monoxide can be synthesized through the vacuum annealing of the graphene oxide multilayer. The effective mass of carriers in GMO is lighter than that of Si[14]. In addition, in a previous study[14], the applied strain can control a lattice parameter and this leads to a change in the band gap of GMO. Due to an easily tunable band gap, GMO may broaden the potential applications in electronics, such as sensors, optoelectronics and transistors.

Because defects govern various characteristics of technological materials like semiconductors, defects fatally influence the electronic properties of crystals[15]. At the same time, defects can be advantageous in some cases[16,17]. In addition, according to the second law of thermodynamics, there is an inevitable disorder in crystalline materials and several defects may be generated during the synthesis or processing[18]. Particularly, vacancies are the main defects derived from the synthesis of carbon nanostructures such as GMOs[19]. Furthermore,

defects can also be deliberately introduced into this material by irradiation or chemical treatments[20,21]. For this reason, it is necessary to investigate how point defects influence GMO, and for application in electronic devices, the change of properties caused by the defects in GMO must also be understood.

In this study, using density functional theory calculations, the possible changes in electronic properties of GMO were investigated referring to formable point defects, such as carbon, oxygen vacancies and interstitial oxygen defect. For this reason, it is necessary to investigate how point defects influence GMO and for application to electronic devices, change of properties by defect in GMO must be understood. In this research, the geometry and electronic structure of GMO, where the point defect appears, will be briefly discussed. By point defects, a reconstructed atom arrangement occurs in GMO. This investigation indicates that the point defects can change the properties of GMO, and the potential application in electronic devices. Furthermore, the electronic band structure of defective GMO is calculated to investigate the change of electronic properties by point defects.

2. Computational details

DFT calculations were performed using the Vienna ab-initio simulation package (VASP) code[22]. The plane-wave basis set was expanded to a cut off energy of 500eV. Projector-augmented waves (PAW)[23] were used to describe the ion cores, and the exchange correlation interactions were expressed with a generalized gradient approximation (GGA)[24,25] in the form of the Perdew, Burke, and Ernzerhof (PBE) functional[26]. All of the self-consistent loops were iterated until the total energy difference of the systems between the adjacent iterating steps became less than 10^{-5}eV. The calculations were performed with a Gamma-point centered 6 × 6 × 1 k-point generated by the Monkhorst-Pack scheme[27]. All the calculations were performed with collinear spin polarization. The simulation model was placed in a 20Å vacuum spacer to avoid interaction between the two adjacent periodic images. The Hellmann-Feynman force on each atom was less than 0.02 eV/Å[28]. Ionic relaxation was executed with the conjugate gradient method.

The lattice parameters of GMO (a_0=3.13Å, α=130˚) are obtained through the lattice parameter optimization (Fig.1.(a)). For the defect calculation, the GMO was modeled as a 4×4 supercell and the defects were induced by removing and adding a single atom through DFT calculations.

3. Results and discussions

The possible point defects and defect formation energies are illustrated in Figure 1. The carbon and oxygen vacancies and the two interstitial oxygen defects of the bridge and hollow sites exclude the on-top site[28], because the oxygen located on the on-top site is in close proximity to the oxygen atom of double-epoxide pair. The defect formation energies (E_f) are calculated for each of the configuration of defective GMO. E_f is defined as:

$$E_f = E_{defect} - E_{perfect} \pm \mu_{atom} \quad (1)$$

where E_{defect} and $E_{perfect}$ are the energies of the defective and perfect GMO, and μ_{atom} is the chemical potential of the isolated atoms (C and $1/2O_2$). The negative sign for the atomic chemical potential (μ_{atom}) is for the case of the oxygen interstitial and the positive sign is for both cases of the oxygen and the carbon vacancy. From an energy point of view, the oxygen vacancy and the interstitial oxygen on the bridge site are more stable to be formed compared to the other two defects, where there is a carbon vacancy and interstitial oxygen at the hollow site (Figure 1(c)). Since the epoxy pair is energetically less stable than the carbonyl pairs[29], the forming of interstitial oxygen on the bridge site needs less formation energy than that of the hollow site. It was also confirmed that the carbon vacancy (the formation energy of 11.02 eV) is hard to form due to the strong covalent bonds of neighboring carbon atoms.

The change in band gap energies for each defect species based on that of perfect GMO indicates how sensitively the electronic properties respond to the local geometric and electronic structure change. In comparison with the band gap of perfect GMO (0.525eV), the band gap of GMO with oxygen vacancy and interstitial oxygen on the hollow site increases to 0.727eV and 0.633eV. However, the band gap of carbon vacancy and interstitial oxygen on

the bridge site decrease to 0.262eV and 0eV. Interestingly, the interstitial oxygen invading the bridge site changes the semiconducting GMO into a metallic GMO. Previously, Pu et al. reported that the band gap of GMO sensitively responds to changes in the opening angle α and increases with a decrease of the opening angle α [14.] In light of the strain effect derived from the change in the opening angle α by defect formation, the local strain field could be generated by defect and affect the electronic properties. The standard definition of the lattice angle is the angle between the lattice vectors in pristine GMO. The defined lattice angle is equal to the angle of the oxygen atoms and the oxygen atoms of the next unit cell (in Figure 1(a)). However, due to the unclear lattice vector of the defective region, the lattice angle of the defective GMO is defined as the angle between the neighboring oxygen atom near the defect and the oxygen atoms of the next unit cell (in Figure 1(c)). The lattice opening angle α of the defective GMO decreases overall from the opening angle of the perfect GMO, except for that of defective GMO with interstitial oxygen on the bridge interstitial site (Table. 1). The tendency of the band gap energy, according to the defect species, is in good agreement with the previous study of the strain effect on band gap energies of GMO[14]. However, since the strain effect is restricted to the area locally formed by a point defect, the band gap energy of this system does not perfectly coincide with the previous study. The increases of the band gap of GMO with an oxygen vacancy and hollow interstitial defect show a similar trend to that of the previous study[14]. However, in contrast to the oxygen vacancy and hollow interstitial defect, the decreases of band gap of carbon vacancy and bridge interstitial defect is discrepant from the trend of the strain effect of GMO. As shown in Figure 2, it is noticed that the band gap of the structures with local tensile strain near the defect (oxygen vacancy and hollow interstitial defect) increases from the band gap of the perfect GMO, and the band gap

of the structures with local compressive strain near the defect (carbon vacancy and bridge interstitial defect) decreases.

The oxygen vacancy creates the dangling bonds toward the missing atom to the neighboring atoms. By the Jahn-Teller effect, which leads to saturation of the dangling bonds, two carbon atoms are connected to each other[18]. Unlike the oxygen vacancy, the dangling bonds caused by the carbon vacancy are unsaturated (in Figure 2.(c)).When the interstitial oxygen atom occupies the hollow site, the interstitial oxygen atom pushes oxygen atoms of double-epoxide pair and it leads to a distorted hexagonal cell of GMO. On the other hand, oxygen adsorption in the bridge site of GMO breaks the double-epoxide pair around the interstitial defect and the interstitial oxygen interacts with carbon atoms of the bridge site. Breaking the double-epoxide bonds causes the oxygen atom to have a remaining dangling bond and it closes with the carbon atom on the opposite bridge site.

Figure 3 shows the effective (unfolded)[30] band structures of defective GMO. In the effective band structure, it seems that the overall outline of the band structure remains except for the defect-induced level and the smearing of the primitive cell eigenvalues. In the unfolded band structure of the perfect supercell (in Figure 3(a)), in principle, the value of the spectral weight (color bar scale) must be integers. However, when using PAW not true Kohn-Sham eigenstates in VASP, the values of the spectral weight deviate slightly from the integers[31]. In the effective band structure[30] of the local tensile strain near the defect, there is no defect-induced level inside the energy gap near the Fermi-level. The change of band gap is caused by the shift of the valence band maximum (VBM) and the conduction band minimum (CBM) in the band structure. In the case of oxygen vacancy (Figure 3(b)), the CBM is shifted upward ~0.15eV and the VBM moves down ~ 0.05eV. In the case of the hollow interstitial (Figure

3(c)), the VBM shows no significant changes, however, the CBM moves upward ~0.12eV. In structures with local tensile strain, the shift of the CBM has a primary influence on the change of band gap and it is analogous to the changing trend of the band structure of GMO on the strain[14]. Briefly, the defect contributions in the alternation of the band gap create the local tensile strain, as stated in the previous study[14]. However, as shown in Table 1, the band gap of structures with a local compressive strain near the defect decreases compared to that of the band gap of perfect GMO. To analyze the change of the band gap, it is necessary to investigate the band structure (Figure 3(d), (e)). The remarkable difference with the perfect band structure is the defect-induced flat band in the band gap. The structures with compressive strain have a dangling bond in common and it leads to the defect-induced level in the effective band structure. In the bridge interstitial, by the dangling bond of oxygen the defect-induced band crosses the Fermi level. The appearance of a band penetrating the Fermi level confirms a metallic property of the system of GMO with bridge interstitial defect. In carbon vacancy, the overall band structure decreases and CBM decreases even further. Additionally, it is considered that the unsaturated dangling bond generated by carbon vacancy in GMO causes defect-induced states. The defect-induced level in the energy gap changes the band gap of structures with a local compressive strain near the defect.

4. **Conclusion**

The geometry and electronic structure of defective GMO was studied systematically using the density functional theory calculations. In terms of defect formation energy of each defective structure, oxygen vacancy and interstitial oxygen on the bridge site were energetically more stable than the other two defects (carbon vacancy and interstitial oxygen on the hollow site). The strain field induced by oxygen vacancy or hollow interstitial oxygen results in local tensile strain near the defects, and the strain field of carbon vacancy and bridge interstitial results in local compressive strain. The band gaps of the defective GMO under local tensile stress are in good agreement with the previous study on the strain effect of GMO on band gap energy. However, interestingly, it was found that the change in the band gap energy of the other defects, such as carbon vacancy or interstitial oxygen on the bridge site, mainly resulted from the unsaturated dangling bond not from the strain effect. Moreover, it was found that the quite sensitive change in band gap energy (from metallic to semiconducting) could be engineered by the defect formation.

Acknowledgement

This research was supported by Basic Science Research Program through the National Research Foundation of Korea (NRF) funded by the Ministry of Education (2013R1A1A2A10064432).

References

1. K. S. Novoselov, A. K. Geim, S. V. Morozov, D. Jiang, Y. Zhang, S. V. Dubonos, I. V. Grigorieva, and A. A. Firsov, Electric Field Effect in Atomically Thin Carbon Films, *Science*, 2004, **306**, 666-669

2. D.Li, R. B. Kaner, Graphene-Based Materials, *Science*, 2008, **320**, 1170–1171.

3. A. K. Geim, K. S. Novoselov, The rise of graphene, *Nat. Mater.*, 2007, **6**, 183–191

4. X. L. Li, X. R. Wang, L. Zhang, S. W. Lee, H. J. Dai, Chemically Derived, Ultrasmooth Graphene Nanoribbon Semiconductors, *Science*, 2008, **319**, 1229–1232

5. Y. G. Semenov, K. W. Kim, J. M. Zavada, Spin field effect transistor with a graphene channel, *Appl. Phys. Lett.*, 2007, **91**, 153105

6. Y. Zhang, T.-T. Tang, C. Girit, Z. Hao, M. C. Martin, A. Zettl, M. F. Crommie, Y. R. Shen, F. Wang, Direct observation of a widely tunable bandgap in bilayer graphene, *Nature*, 2009, **459**, 820-823

7. S. B. Cho, Y.-C. Chung, Bandgap engineering of graphene by corrugation on lattice-mismatched MgO (111), *J. Mater. Chem. C*, 2013, **1**, 1595-1600

8. Y. Qi, S. H. Rhim, G. F. Sun, M. Weinert, L. Li, Epitaxial Graphene on SiC(0001): More than Just Honeycombs, *Phys. Rev. Lett.*, 2010, **105**, 085502.

9. M. Y. Han, B. Ozyilmaz, Y. B. Zhang, P. Kim, Energy Band-Gap Engineering of Graphene Nanoribbons, *Phys. Rev. Lett.*, 2007, **98**, 206805

10. X. R. Wang, H. J. Dai, Etching and narrowing of graphene from the edges, *Nat. Chem.*, 2010, **2**, 661–665

11. L. A. Ponomarenko, F. Schedin, M. I. Katsnelson, R. Yang, E. W. Hill, K. S. Novoselov, A. K. Geim, Chaotic Dirac Billiard in Graphene Quantum Dots, *Science*, 2008, **320**, 356–358.

12. X. R. Wang, X. L. Li, L. Zhang, Y. Yoon, P. K. Weber, H. L. Wang, J. Guo and H. J. Dai, N-Doping of Graphene Through Electrothermal Reactions with Ammonia, *Science*, 2009, **324**, 768–771

13. E. C. Mattson, H. H. Pu, S. M. Cui, M. A. Schoeld, S. Rhim, G. H. Lu, M. J. Nasse, R. S. Ruo, M. Weinert, M. Gajdardziska-Josifovska, J. H. Chen, C. J. Hirschmugl, Evidence of Nanocrystalline Semiconducting Graphene Monoxide during Thermal Reduction of Graphene Oxide in Vacuum, *ACS Nano*, 2011, **5**, 9710–9717.

14. H. H. Pu, S. H. Rhim, C. J. Hirschmugl, M. Gajdardziska-Josifovska, M. Weinert, J. H. Chen, Strain-induced band-gap engineering of graphene monoxide and its effect on graphene, *Phys. Rev. B*, 2013, **87**, 085417

15. C. Kittel, Introduction to solid state physics, 8th ed., John Wiley & Sons: New York, 2005

16. D. J. Appelhans, Z. Lin, M.T.Lusk, Two-dimensional carbon semiconductor: Density functional theory calculations, *Phys. Rev. B*, 2010, **82**, 073410

17. J.Kotakoski, A.V.Krasheninnikov, U.Kaiser, J.C.Meyer, From Point Defects in Graphene to Two-Dimensional Amorphous Carbon, *Phys. Rev. Lett*., 2011, **106**, 105505

18. F. Banhart, J. Kotakoski, A.V. Krasheninnikov, Structural defects in graphene, *ACS Nano*, 2011, **5**, 26-41

19. A.V. Krasheninnikov, F. Banhart, Engineering of nanostructured carbon materials with electron or ion beams, *Nat. Mater.*, 2007, **6**, 723-733

20. F. Banhart, T.Fuller, Ph.Redlich, P.M. Ajayan, The formation, annealing and self-compression of carbon onions under electron irradiation. *Chem. Phys. Lett.*, 1997, 269, 349-355

21. K.Urita, K.Suenaga, T. Sugai, H. shinohara, S.Iijima, In Situ Observation of Thermal Relaxation of Interstitial-Vacancy Pair Defects in a Graphite Gap, *Phys. Rev. Lett*., 2005, **94**, 155502

22. G. Kresse, J. Furthmuller, Efficient iterative schemes for ab initio total-energy calculations using a plane-wave basis set, *Phys. Rev. B*, 1996, **54**, 11169.

23. P. E. Blochl, Projector augmented-wave method, *Phys. Rev. B*, 1994, **50**, 17953

24. J. P. Perdew, J. A. Chevary, S. H. Vosko, K. A. Jackson, M. R. Pederson, D. J. Singh, C. Fiolhais, Atoms, molecules, solids, and surfaces: Applications of the generalized gradient approximation for exchange and correlation, *Phys. Rev. B*, 1992, **46**, 6671

25. J. P. Perdew, Y. Wang, Accurate and simple analytic representation of the electron-gas correlation energy, *Phys. Rev. B*, 1992, **45**, 13244

26. J. Perdew, K. Burke, M. Ernzerhof, Generalized Gradient Approximation Made Simple, *Phys. Rev. Lett.*, 1996, **77**, 3865–3868.

27. H. Monkhorst, J. Pack, Special points for Brillouin-zone integrations, *Phys. Rev. B*, 1976, **13**, 5188–5192

28. A. Ishii, M. Yamamoto, H. Asano, K. Fujiwara, DFT calculation for adatom adsorption on graphene sheet as a prototype of carbon nanotube functionalization, *J. Phys.: Conf. Ser.*, 2008, **100**, 052087

29. W. H. Zhang, V. Carravetta, Z. Y.Li, Y. Luo, J. L. Yang, Oxidation states of graphene: Insights from computational spectroscopy, *J. Chem. Phys.*, 2009, **131**, 244505

30. P. V. C. Medeiros, S.Stafstrom, J.Bjork, Effects of extrinsic and intrinsic perturbations on the electronic structure of graphene: Retaining an effective primitive cell band structure by band unfolding, *Phys. Rev. B*, 2014, **89**, 041407(R)

Figure Captions

Figure 1. Schematic view of the point defects of GMO. Carbon and oxygen atoms are colored gray and red, respectively. (a) Structure of GMO and structural parameters of GMO are labeled. (b) Arbitrary directions (upper or lower) from one of neighboring oxygen atoms around the defect in Table 1 are labeled. (c) Configuration of defective GMO and formation energy of defective GMO. Blue dash and red circle in configuration is the position of interstitial defect and vacancy. Lattice opening angle α of defective GMO is labeled.

Figure 2 Relaxed structures of GMO and strain field near the defect. (a) Perfect GMO, GMO with (b) oxygen vacancy, (c) carbon vacancy, (d) oxygen hollow interstitial defect, (e) oxygen bridge interstitial defect. The atomic bonding lengths are colored according to the increase (red), or decrease (blue) from the bonding length of perfect GMO. The atomic bonds are colored according to the color bar in the variation of the bond length between defective GMO and perfect GMO.

Figure 3 (unfolded) band structure of perfect and defective GMO(a) Perfect GMO. GMO with (b) oxygen vacancy, (c) oxygen hollow interstitial defect (d) carbon vacancy, (e) oxygen bridge interstitial defect The scale of the color bar below the band structure is the number of primitive cell bands crossing the interval (0.05eV) at a given primitive wave-vector. Inset figure is the schema of high symmetry points in Brillouin zone.

		Perfect		Oxygen vacancy		Carbon vacancy		Bridge interstitial		Hollow interstitial	
		$d_{o\text{-}o}$(Å)	α(°)	$d_{o\text{-}o}$(Å)	α(°)	$d_{o\text{-}o}$(Å)	α(°)	$d_{o\text{-}o}$(Å)	α(°)	$d_{o\text{-}o}$(Å)	α(°)
Direction	Upward*	2.64	130.0	2.71	128.5	2.63	129.9	2.59	130.7	2.66	129.6
	Downward*	2.64	130.0	2.75	128.5	2.69	128.8	2.72	127.7	2.61	129.3
band gap(eV)		0.525		0.727		0.261		0.000		0.633	

Table 1 Structural parameters around defects and band gaps of defective GMO. Upward* is arbitrary direction from most neighboring oxygen atom near the defect. Downward* is opposite direction of Upward*.

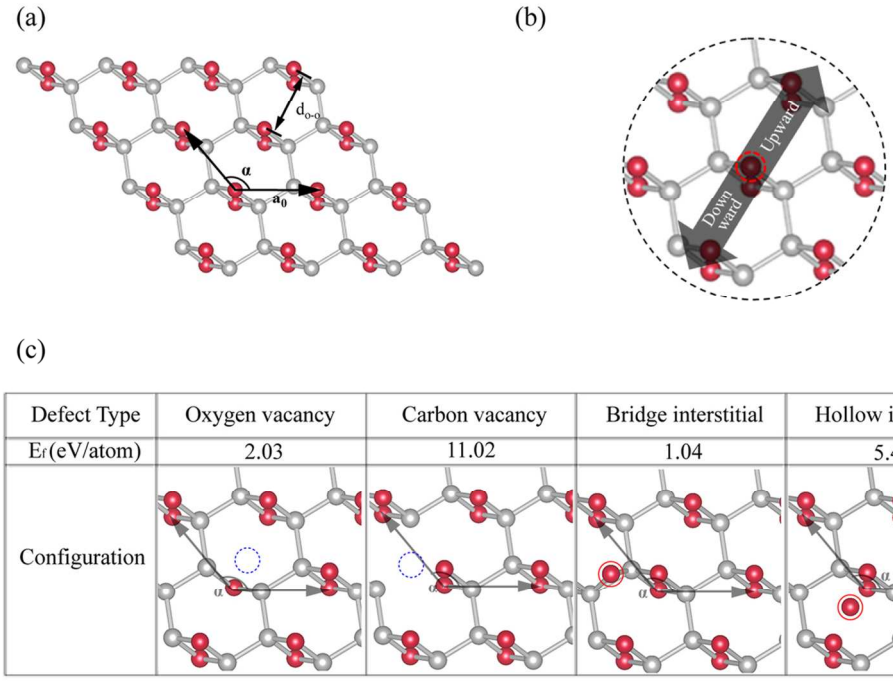

Defect Type	Oxygen vacancy	Carbon vacancy	Bridge interstitial	Hollow interstitial
E_f(eV/atom)	2.03	11.02	1.04	5.45
Configuration				

Figure 1. Schematic view of the point defects of GMO. Carbon and oxygen atoms are colored gray and red, respectively. (a) Structure of GMO and structural parameters of GMO are labeled. (b) Arbitrary directions (upper or lower) from one of neighboring oxygen atoms around the defect in Table 1 are labeled. (c) Configuration of defective GMO and formation energy of defective GMO. Blue dash and red circle in configuration is the position of interstitial defect and vacancy. Lattice opening angle α of defective GMO is labeled.
116x79mm (300 x 300 DPI)

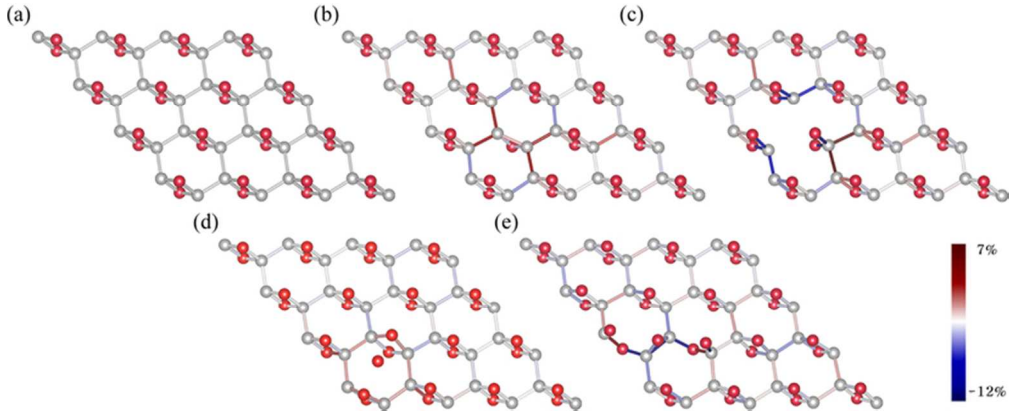

Figure 2 Relaxed structures of GMO and strain field near the defect. (a) Perfect GMO, GMO with (b) oxygen vacancy, (c) carbon vacancy, (d) oxygen hollow interstitial defect, (e) oxygen bridge interstitial defect. The atomic bonding lengths are colored according to the increase (red), or decrease (blue) from the bonding length of perfect GMO. The atomic bonds are colored according to the color bar in the variation of the bond length between defective GMO and perfect GMO.
69x28mm (300 x 300 DPI)

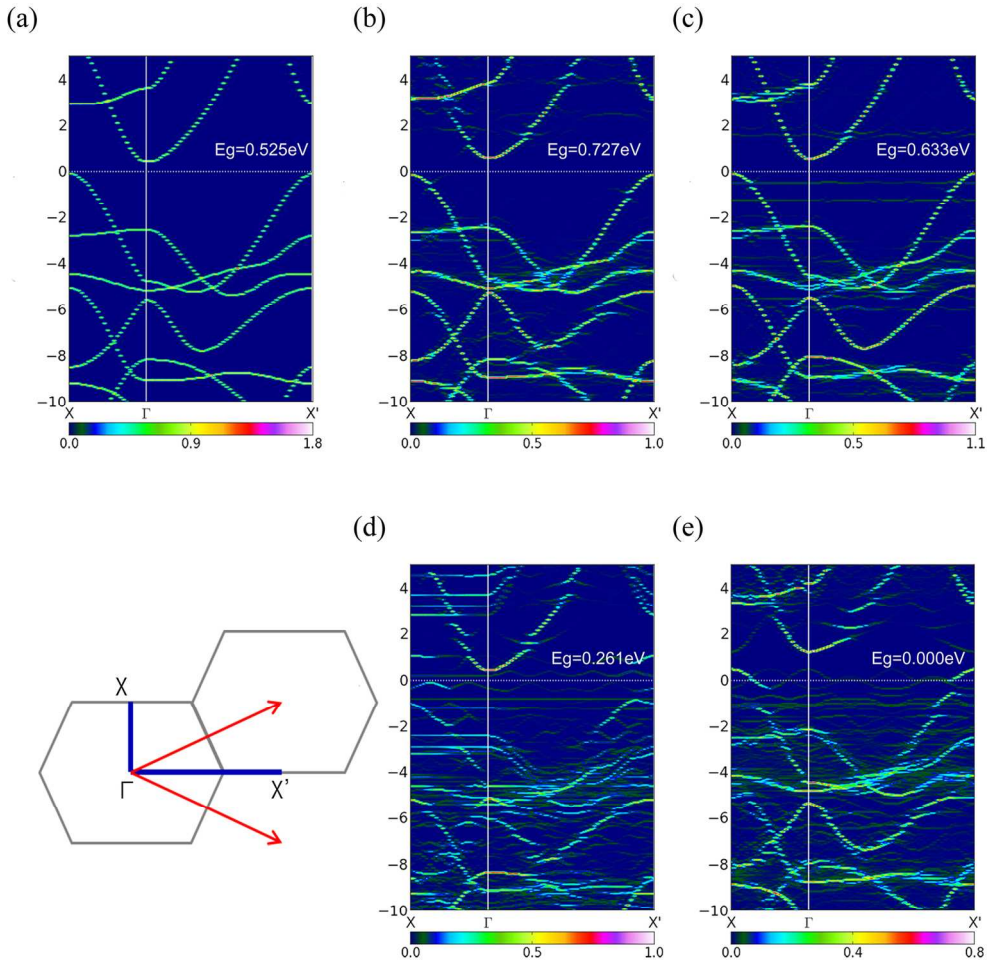

Figure 3 (unfolded) band structure of perfect and defective GMO(a) Perfect GMO. GMO with (b) oxygen vacancy, (c) oxygen hollow interstitial defect (d) carbon vacancy, (e) oxygen bridge interstitial defect The scale of the color bar below the band structure is the number of primitive cell bands crossing the interval (0.05eV) at a given primitive wave-vector. Inset figure is the schema of high symmetry points in Brillouin zone.
171x171mm (300 x 300 DPI)